Basic structures of the Shilnikov homoclinic bifurcation scenario

Rene O. Medrano-T.,[a] Murilo S. Baptista, and Iberê L. Caldas
Instituto de Física, Universidade de São Paulo, C. P. 66318, CEP 05315-970 São Paulo, SP, Brazil

(Received 13 April 2004; accepted 8 July 2005; published online 16 September 2005)

We find numerically small scale basic structures of homoclinic bifurcation curves in the parameter space of the Chua circuit. The distribution of these basic structures in the parameter space and their geometrical properties constitute a complete homoclinic bifurcation scenario of this system. Furthermore, these structures and the scenario are theoretically demonstrated to be generic to a large class of dynamical systems that presents, as the Chua circuit, Shilnikov homoclinic orbits. We classify the complexity of primary and subsidiary homoclinic orbits by their order given by the number of their returning loops. Our results confirm previous predictions of structures of homoclinic bifurcation curves and extend this study to high order primary orbits. Furthermore, we identify accumulations of bifurcation curves of subsidiary homoclinic orbits into bifurcation curves of both primary and subsidiary orbits. © *2005 American Institute of Physics*.
[DOI: 10.1063/1.2031978]

Shilnikov homoclinic orbits are trajectories that depart from a fixed saddle-focus point, with specific eigenvalues, and return to it after an infinity time (that is also true to time reversal evolution). Since they are intimately connected to the existence of chaos and the existence of a countable infinity of periodic orbits, it is important to understand their bifurcation in the parameter space. Such homoclinic orbits are connected to the chaotic dynamics of systems of different areas, as chemical chaos,[1] glow-discharge systems,[2] spiking neurons,[3,4] rabbit arteries intermittency,[5] noise-induced phenomena,[6] and such electrochemical oscillators.[7] Here, we find numerically the basic codimension-one structure of the bifurcation curves of these orbits analyzing the parameter space of the Chua circuit. We demonstrate its generality by constructing such structure theoretically from a two-parameter bifurcation analysis performed in a generic normal form of dynamical systems that have a Shilnikov homoclinic orbit. The set of the identified basic bifurcation curve structures forms a scenario that can guide researchers to find, in the parameter space, accumulation of chaotic sets, periodic orbits, and horseshoes for systems with Shilnikov homoclinic orbits.

I. INTRODUCTION

Homoclinic orbits, chaos, and periodic orbits are closely connected. This connection was first noticed in the end of the XIX century, when Poincaré was studying the solvability of the equations of the three-body problem. He showed the impossibility of solving these equations due to the existence of homoclinic orbits and the sensitivity to initial conditions, the most important trademark of chaotic behavior. The relation between chaos and periodic orbits was demonstrated in the sixties, when Smale showed that the existence of a horseshoe, an invariant set that contains an infinity number of periodic orbits in a discrete chaotic system,[8] implies chaos. Soon later, Shilnikov[9] showed that, for a class of time-continuous three-dimensional dynamical systems, the existence of a Shilnikov homoclinic orbit (the joint of the stable and unstable manifolds of a saddle-focus fixed point with specified eigenvalues) implies the existence of a horseshoe in the neighborhood of this orbit, and therefore, chaos.

After that, a series of numerical and experimental investigations revealed how the Shilnikov homoclinic orbits in the vicinity of a chaotic attractor determine its dynamical and topological properties[1,10]. More recent works[11–17] have extended the Shilnikov results and demonstrated that the existence of one Shilnikov homoclinic orbit implies the existence of infinite homoclinic orbits.

A homoclinic bifurcation occurs for some parameters if there is a homoclinic orbit for these parameters. Each homoclinic bifurcation curve describes a family of homoclinic orbits in the parameter space. One-parameter local bifurcation analysis in the neighborhood of a Shilnikov homoclinic orbit showed that there exists an infinite number of other subsidiary homoclinic orbits associated with that primary one, each one with its countable infinity of horseshoes.[15]

Then, given a primary Shilnikov homoclinic orbit, the existence of other Shilnikov subsidiary orbits of arbitrary order was demonstrated (see Ref. 16) (defined as the number of loops through phase space before returning to the equilibrium fixed point). In Ref. 17 a two-parameter space analysis was presented predicting the distribution of two structures of homoclinic bifurcation diagrams of subsidiaries H_2 and H_3 nearby a primary H_1 parameter. A conjecture is also presented about the increasing complexity of other structures containing bifurcation curves with order $n>3$. After that, in a recent work[18] we derived a general scaling law that gives the ratio between bifurcation parameters of different nearby Shilnikov orbits in parameter space. These analytical results were numerically confirmed in the parameter space of Chua circuit.[19]

[a]Electronic mail: rmedrano@if.usp.br

Our present work deals with the numerical identification of basic structures formed by the bifurcation curves of the Chua circuit[20] in the parameter space. These structures involve accumulation of bifurcation curves of subsidiary H_{nj} orbits $(n>1)$ into both primary homoclinic orbits, H_j, (of any order $j \in \mathbb{N}^*$) and other subsidiaries. The representation of these basic structures in the physical control parameters is analytically deduced by a two-parameter analysis performed for dynamical systems, in a normal form, that presents Shilnikov homoclinic orbits. Thus, this analytical result and the numerical homoclinic bifurcation codimension-one scenario obtained for the Chua parameter space are valid for to a large class of dynamical systems. Here, we classify the Shilnikov orbits, H_m, by their order, m, defined by the number of loops they described in phase space. These orbits predicted in our work could also be discriminated according to the number of circuits around the unstable direction as was done in Ref. 17. Basic structures similar to those reported in this work were predicted before, in Ref. 17, for orbits with a high number of circuits. Differences in the described structures are due to the different parameter spaces used in these works. In our case we looked for physical control parameters such that the predicted bifurcations could be identified in experiments involving the Chua circuit. On the other hand, in Ref. 17 general statements were derived for homoclinic bifurcation curves with a large variation in terms of a saddle index, a parameter obtained from the saddle eigenvalues.

This paper is organized as follows. Since all our numerical work is performed on the Chua circuit, we present in Sec. II a short description of this dynamical system, its phase space topology, and its main attractors in phase and parameter space. In Sec. III, we show examples of homoclinic orbit families observed in the Chua circuit, and present a two-parameter characterization of the trajectories leaving the saddle focus as a way to understand the homoclinic bifurcations. In Sec. IV, we perform the same two-parameter analysis to reveal the generic structure of the bifurcation curves of the Chua circuit and present the theoretical model for the microscopic structure of the family bifurcations. Finally, in Sec. V we present the conclusions.

II. CHUA CIRCUIT AND ITS ATTRACTORS

The Chua circuit is schematically shown in Fig. 1(a). It is composed of two capacitors, C_1 and C_2, one linear resistor, R, one inductor, L, and the nonlinear negative resistor, R_N, whose characteristic curve, a piecewise-linear function, is represented in Fig. 1(b). The rescaled Chua circuit equations in dimensionless units[20] are

$$\dot{x}' = \alpha[y' - x' - k(x')],$$

$$\dot{y}' = x' - y' + z',$$

$$\dot{z}' = -\beta y',$$

$$k(x') = bx' + \tfrac{1}{2}(a-b)(|x'+1| - |x'-1|) \qquad (1)$$

and we set $a=-8/7$ and $b=-5/7$; α and β are control parameters.

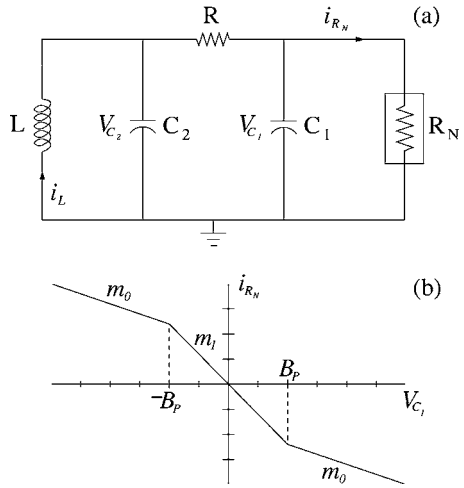

FIG. 1. (a) Representation of the Chua circuit, with two capacitors, C_1 and C_2, one inductor L, and one linear resistor R. R_N is a piecewise linear negative resistor whose characteristic curve is shown in (b).

In Fig. 2 we show a bidimensional projection on the variables x' and y' of four of the possible three-dimensional attractors such circuit presents. In Figs. 2(a) and 2(b) stable periodic attractors, period-1 and period-2, respectively, and in Figs. 2(c) and 2(d) chaotic attractors, the Rössler-type one and the double-scroll one, respectively, are shown.

The phase space of Eq. (1) has three domains: $D_0 = \{\mathbb{R}^3 \| x' | \leqslant 1\}$, $D_+ = \{\mathbb{R}^3 | x' \geqslant 1\}$ and $D_- = \{\mathbb{R}^3 | x' \leqslant -1\}$. There is a fixed point in each domain: $P_0 = (0,0,0)$, in D_0, and $P_\pm = (\pm\ell, 0, \mp\ell)$, in $D_\pm$, where $\ell = (b-a)/(b+1) = 1.5$. These points are indicated in Figs. 2(a)–2(d) with the presented attractors.

The way periodic attractors and chaotic attractors appear as we vary the parameters α and β can be visualized in the parameter space of Fig. 3, where we indicate with gray levels the parameters for which we have each one of the three types of attractors: periodic, Rössler-type, and double scroll. As one shall see, most of the homoclinic orbits presented here coexist in parameter space with the double scroll attractor.

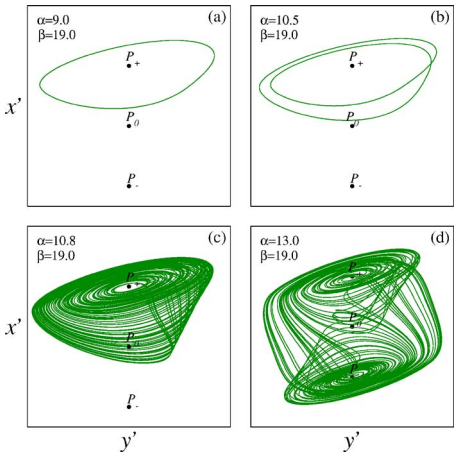

FIG. 2. Four possible attractors from Eq. (1). (a) Stable period-1 attractor, (b) stable period-2 attractor, (c) chaotic Rössler-type attractor, and (d) chaotic double scroll attractor. The fixed points are indicated by P_+, P_0, and P_-.

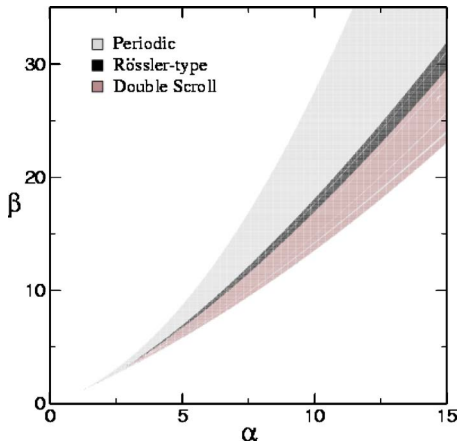

FIG. 3. Parameter space with the regions where we find periodic attractors (light gray), Rössler-type attractors (black), and double scroll attractors (dark gray).

In this work, we are interested in homoclinic orbits to the saddle-focus fixed point P_0. For this point, the Jacobian matrix of Eq. (1) has a pair of complex conjugate eigenvalues $-\rho \pm i\omega$ that determine the bidimensional stable subspace, $E^S(P_0)$, tangent to the stable manifold in the vicinity of P_0. It has also a real eigenvalue λ, that determines the one-dimensional unstable subspace $E^U(P_0)$, which coincides with the one-dimensional unstable manifold, in D_0. A more complete geometrical description of the system can be seen in Fig. 4; more details are in Ref. 19 where we have also described the conditions for the existence of a homoclinic orbit to the point P_0.

In an order-n,m homoclinic orbit of P_0, n and m means that this orbit turns n times around the fixed point P_+, and m times around the fixed point P_-. To find homoclinic orbits $H_{n,0}$, we introduce a measure $d_{n,0}$, the distance between the line L_+ and the point $Q_{n,0}$ (indicated in Fig. 4 for $n=1$). $Q_{n,0}$ is the intersection of the unstable manifold of P_0 with the plane U_+ (Fig. 4), when the flow goes to D_0 after n turns around P_+. We consider $d_{n,0}>0$ if $Q_{n,0}$ is between L_+ and the axis x', and $d_{n,0}<0$ if L_+ is between $Q_{n,0}$ and the axis x'. Whenever $m=0$, we will omit this index. Thus, in Fig. 4 we represent $d_{1,0}$ ($n=1$ and $m=0$) as d_1, and $Q_{1,0}$ as Q_1. Similarly, to find homoclinic orbits $H_{n,m}$ we introduce the distance $d_{n,m}$ in the plane U_-. Finding an order-n,m orbit, $H_{n,m}$, is equivalent to finding a parameter for which $d_{n,m}=0$.

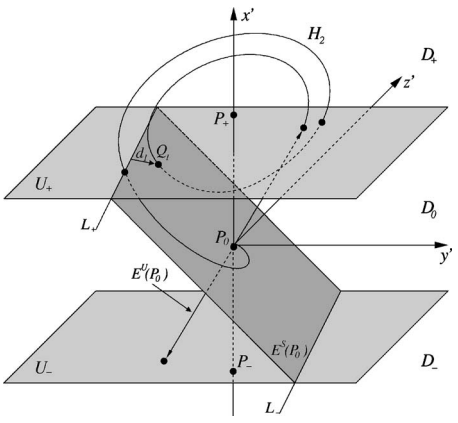

FIG. 4. Fixed point P_0 with its stable and unstable subspaces $E^S(P_0)$ and $E^U(P_0)$. The term d_1 is the distance between Q_1 and the line L_+ on the plane U_+. The term $d_2=0$, so there is a homoclinic orbit H_2, whose trajectory turns two times around the fixed point P_+. The plane $U_\pm=\{\mathbb{R}^3 | x=\pm 1\}$ is the boundary of the domains D_0 with $D_\pm$. In D_0, $E^S(P_0)$ is a plan and $E^U(P_0)$ is a line, both limited by U_+ and U_-. So, $L_\pm=E^S(P_0)\cap U_\pm$.

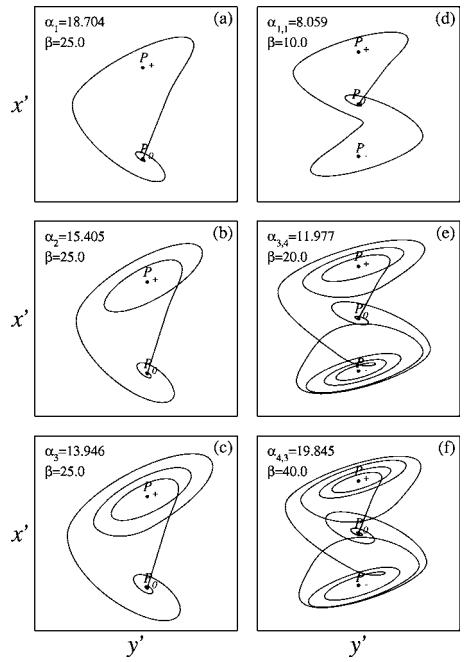

FIG. 5. A series of homoclinic orbits of different orders: $n=1$ (a), $n=2$ (b), $n=3$ (c), $n,m=1,1$ (d), $n,m=3,4$ (e), $n,m=4,3$ (f). The parameters α and β are indicated in the figure.

In Figs. 5(a)–5(f) we show a series of homoclinic orbits of different orders: $n=1$ (a), $n=2$ (b), $n=3$ (c), $n,m=1,1$ (d), $n,m=3,4$ (e), $n,m=4,3$ (f). As already conventioned, the index $m=0$ is omitted in (a),(b),(c). The high order orbit geometry already looks similar to the chaotic attractor geometry.

According to the Shilnikov theorem, if a homoclinic orbit exists, and the eigenvalues satisfy the condition $\delta<1$, with $\delta=|\rho/\lambda|$, there exists a countable number of infinity Smale horseshoes in the vicinity of the homoclinic orbit.[9] In Fig. 6, the dashed lines correspond to parameter values for which the Shilnikov condition, $\delta<1$, is satisfied and the light gray region corresponds to $\delta>1$. In the dark gray region the Shilnikov theorem cannot be applied because the eigenvalues ρ and λ are in $\mathbb{R}$. Most homoclinic orbits studied in this work have parameters within the region where $\delta<1$, except for some H_1 orbits near the origin of the parameter space.

III. HOMOCLINIC BIFURCATIONS

A codimension-one bifurcation curve in the bidimensional parameter space $\beta\times\alpha$ defines a family of homoclinic orbits $H_{n,m}$. This continuous curve in parameter space represents a set of infinity parameter values for which orbits $H_{n,m}$ exist. The structure formed by the bifurcation curves in the parameter space constitutes the scenario we obtain in this work.

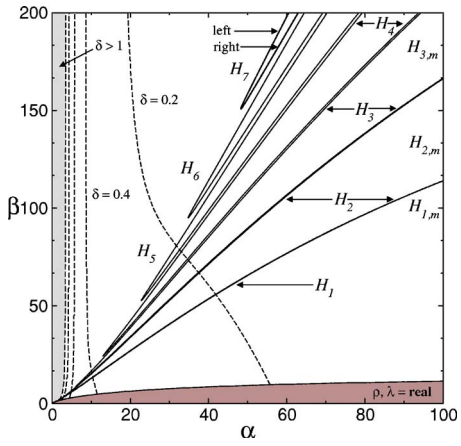

FIG. 6. Parameter space of the primary homoclinic orbits H_n, with $n=1,\ldots,7$. Dashed lines correspond to parameters values for which the Shilnikov condition is satisfied. Shilnikov conditions are not satisfied in light and gray regions.

Examples of homoclinic bifurcation curves are shown in Fig. 6, in which it is possible to observe the first primary families[21] of orbits H_j, with $j=1,\ldots,7$ ($m=0$). With the exception of the bifurcation curve of the H_1 family, all the other bifurcation curves (orders varying from 2 to 7) have two branches, left and right, as indicated for the family-H_7 curve in Fig. 6. For parameters within each region bounded by a primary H_j bifurcation curve there are no H_n orbits. This is a consequence of the fact that, for parameters in that region, any trajectory leaving the point P_0 goes to the domain D_-, and therefore, only families of the type $H_{j,m}$, with $m>0$ can exist. So, we find the family-$H_{j,m}$ within these regions. H_n subsidiary orbits appear between the right branch of an order-$(j+1)$ orbit and the left branch of an order-j orbit.

Next, we present typical properties of homoclinic orbit bifurcation curves in a small part of the parameter space shown in Fig. 6. However, these properties are general and can be observed in other areas of the parameter space.

Initially, we show in Fig. 7(a) an example of a primary-H_3 family curve and the corresponding orbit. To understand the bifurcation scenario from which this family appears in parameter space, in Fig. 7(b) we show the distance d_3 as the parameter α is increased and β is kept fixed. The distance d_3 is unimodal, presents one local minimum and vanishes twice, so in the parameter space of Fig. 7(a) we observe two orbits H_3 for that fixed β. As we decrease β, the minimum of d_3

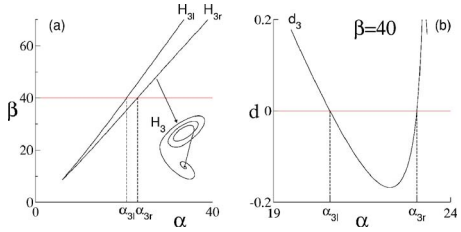

FIG. 7. (a) Primary family-H_3 curve in the parameter space $\beta\times\alpha$ and a H_3 orbit indicated by the arrow. (b) The d_3 function with respect to α, $\beta=40$. Homoclinic orbits of the family-H_3 exist when $d_3=0$.

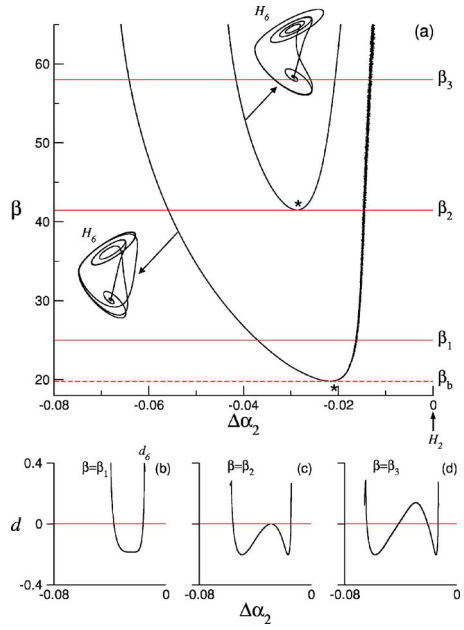

FIG. 8. (a) Two subsidiary family-H_6 curves and (b)–(d) d_6 function with respect to $\Delta\alpha_2=\alpha-\alpha_2$ for β_1, β_2, and β_3 indicated by the lines in (a), and α_2 is the parameter for which an orbit H_2 (indicated by the arrow in the origin) is formed ($\Delta\alpha_2=0$). Homoclinic orbits of the family-H_6 exist when $d_6=0$. β_b is the local minimum of the longer family-H_6 curve.

increases until d_3 does not vanish and there is no homoclinic orbit.

As shown in Ref. 18 the vicinity of the primary family-H_3 curve, shown in Fig. 7, contains an infinity number of subsidiary family-H_6 curves. The distance d_6 vanishes an infinity number of times, as $\alpha\to\alpha_{3_r}$ for a decreasing α, and as $\alpha\to\alpha_{3_l}$ for an increasing α.

Now, we show in Fig. 8(a) two bifurcation curves, of subsidiary H_6 orbits, which are localized between the bifurcation curves of the primary orbits H_2 and H_3, shown in Fig. 6. In Figs. 8(a)–8(d) we show the distance d_6, for the values β_1, β_2, and β_3, indicated by lines in 8(a), as we vary $\Delta\alpha_2=\alpha-\alpha_2$, with α_2 being the α value for which H_2 exists. Differently from what is observed in Fig. 7(a) for a primary orbit curve, in Fig. 8(a) we observe that one subsidiary H_6 curve is within another subsidiary H_6 curve. We see that d_6 in Fig. 8(b) is a unimodal function, as in Fig. 7(a), with a local minimum crossing twice the $d=0$ line. As we increase β another family-H_6 appears, when d_6 in Fig. 8(c) has two local minima and one local maximum, presenting tree values of $\Delta\alpha_2$ for which $d_6=0$. Then, for $\beta=\beta_3$, the d_3 function has four values for which $d_6=0$.

The two-parameter character of this bifurcation is present in the appearance of local maxima or minima in the d function versus α as we change the parameter β. That character is responsible for creating other homoclinic orbits in the vicinity of α parameters for which an orbit already exists.

We present bifurcation curves of primary [Fig. 8(a)] and subsidiary [Fig. 7(a)] homoclinic orbits in the parameter space. However, we find an accumulation of subsidiary family orbits into these curves. Thus, in the regions between two primary bifurcation curves there are always parameters for

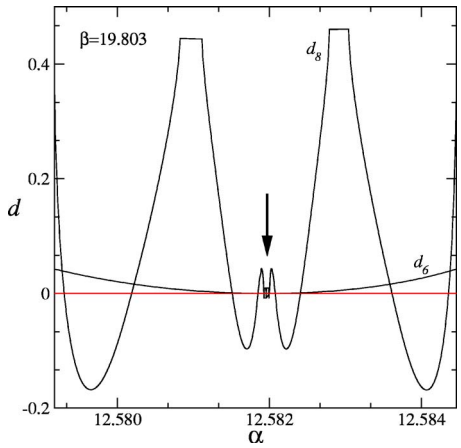

FIG. 9. The d_6 and d_8 functions with respect to α for $\beta=19.803$. The arrow shows the local minimum of d_6 at $\alpha^* \approx 12.582$; d_6 is always positive. There is an outer accumulation of orbits H_8 into the orbit H_6.

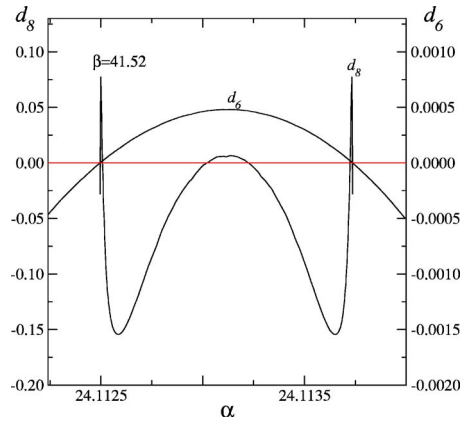

FIG. 10. The d_6 and d_8 functions with respect to α, for $\beta=41.52$, showing the inner accumulation of orbits H_8 into the orbit H_6.

which subsidiary orbits exist, although they are not shown in Fig. 6.

In short, the structure of the bifurcation curves can be pictorially described as being formed by a within-to-within accumulation of subsidiary families into other subsidiary or primary families. The bifurcation scenario of the parameter accumulations can be studied by a one-parameter approach of subsidiary order-nj orbits (H_{nj}) into order-$(n-1)j$ orbits ($H_{(n-1)j}$), in the vicinity of H_j ($n,j \in \mathbb{N}$ with $n \geqslant 2$ and $j \geqslant 1$). To see this, we analyze the homoclinic bifurcations for β values close to those indicated by stars in Fig. 8(a), at the bottom point of each family-H_6 curve.

In Fig. 9 we show the distances d_6 and d_8 vs α for $\beta=19.803<\beta_b$ [β_b is indicated in Fig. 8(a)]. There are H_8 orbits for $d_8=0$; d_6 is positive and close to zero. Although an orbit H_6 does not exist, it is possible to recognize the accumulation of subsidiary H_8 ($n=4,j=2$) orbits into the d_6 minimum where the subsidiary H_6 ($n-1=3,j=2$) orbit will appear for $\beta=\beta_p$. This accumulation happens in the vicinity of the primary H_2 ($n=1,j=2$) whose critical parameter was used as a reference in 8. The minimum for d_6 is in $\alpha^* \approx 12.582$. As we vary α approaching α^*, d_8 becomes zero several times. Assuming the index i and $i+1$ to describe two consecutive α values for which $d_8=0$, the distance $|\alpha^i - \alpha^{i+1}|$ shrinks as α approaches α^*. The index i increases in the direction of α^* with an accumulation of α^i values on α^*. Thus, as β reaches β_b, d_6 vanishes once and d_8 vanishes several times, for $\alpha \approx \alpha^*$. So, there is an accumulation of family-H_8 curves into the family-H_6 curves, from outside the external curve of Fig. 8(a). So we refer to this accumulation process as an outer accumulation. Note that if $\beta \gtrsim \beta_b$, for example $\beta=\beta_1$, d_6 becomes smaller than zero inside the H_6 bifurcation curve, and thus, no H_8 orbit is observed in this region.

A similar accumulation process is in Fig. 10, in which we show the distances d_6 and d_8 vs α for $\beta=41.52>\beta_2$ [where β_2 is the minimum β of the internal family curve in Fig. 8(a)]. In this figure, the left vertical axis represents d_8 and the right vertical axis d_6. In this figure, there are two zones of accumulation, where d_6 is close to zero and positive. As α approaches the values for which $d_6=0$ (orbit H_6 exists), d_8 vanishes several times. We refer to this accumulation process as an inner accumulation, as it happens in Fig. 8(a), for parameters between the two H_6 curves.

These inner and outer accumulations are verified along the two family-H_6 curves. Although only shown for a family-H_6, these results can be extended to families of any order for similar conditions in the neighborhood of a primary or a subsidiary family curve. To know if the accumulation process of a family-H_{nj} into a family-$H_{(n-1)j}$ is either of type outer or inner, all we need is to verify if the $d_{(n-1)j}$ function has either a local minimum (as in Fig. 9) or a local maximum (as in Fig. 10). In Fig. 11 we represent these types of accumulation process.

In Fig. 11(a) we represent one structure of bifurcation curves in the vicinity of subsidiary family curves. Between two subsidiary family-H_{nj} curves, one within the other, there is an outer accumulation process of the curves $H_{(n+1)j}$ into the internal family-H_{nj} curve, and an inner accumulation process of the family-$H_{(n+1)j}$ curves into the external family-H_{nj} curve. These accumulations are represented in Fig. 11(a) by

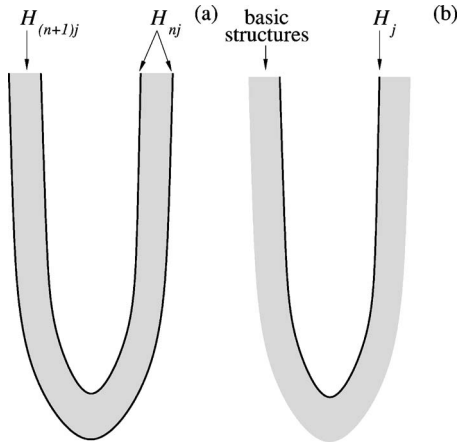

FIG. 11. Representation of basic structures of the homoclinic bifurcation curves in the Chua circuit parameter space. (a) Basic structure of the inner and outer accumulation of subsidiary family-$H_{(n+1)j}$ curves inside two family-H_{nj} curves. (b) The outer accumulation of basic structure curves into a primary family-H_j curve.

the gray region. From this basic structure, we can construct the more complex structures observed in the homoclinic bifurcations of the Chua parameter space. For example, one can consider that the two family-H_{nj} curves like the ones shown in Fig. 11(a) are accumulating into a family-$H_{(n-1)j}$ that is somewhere within these two family-H_{nj} curves. Thus, what we see are infinities replications of the structure seen in Fig. 11(a) one inside the other (in the blank region) as one approaches the family-$H_{(n-1)j}$ curve. With the constraint that, between two family-H_{nj} curves, there is a region where no family-H_m curves are found, with $m \in \mathbb{N}$. Moreover, similar replications can be found in the gray region involving $H_{(n+2)j}$ accumulating into $H_{(n+1)}$.

In Fig. 11(b) we show the structure in the vicinity of a primary family curve. As previously discussed, in the Chua circuit, the d_j functions for all the observed primary family-H_j is only positive between the left branch of the family-H_j curve and the right branch of the family-H_{j+1} curve. Thus, around the primary family curves, the accumulation process, family-H_{2j} into family-H_j, is always of the outer type. One can pictorially visualize this scenario as having in the gray region of Fig. 11(b) an infinity number of basic structures of the type shown in Fig. 11(a).

IV. BIFURCATION SCENARIO

The theoretical description of the codimension-one bifurcation curves in parameter space is done by an extension of the one-parameter bifurcation analysis performed in Ref. 18. To achieve that, we first derive a map that captures the evolution of trajectories departing from a saddle-focus point.[18] With this map we vary one parameter to understand the distance d variation observed in Figs. 7(b) and 8(b)–8(d).

The simplified dynamics of a system that has a Shilnikov homoclinic orbit is given, in the vicinity of this orbit, by the following normal form:

$$\begin{aligned} \dot{x} &= \rho x - \omega y + P(x,y,z;\mu), \\ \dot{y} &= \omega x + \rho y + Q(x,y,z;\mu), \\ \dot{z} &= \lambda z + R(x,y,z;\mu), \end{aligned} \tag{2}$$

where the eigenvalues of the saddle-focus fixed point are $\lambda_1=\lambda$ and $\lambda_{2,3}=\rho\pm i\omega$, with $\lambda\rho<0$ and $\omega\neq 0$. The functions P, Q, and R are real analytics, and $\dot{P}(0,0,0;\mu)=\dot{Q}(0,0,0;\mu)=\dot{R}(0,0,0;\mu)=0$, for the fixed point in the origin; μ is a control parameter. If there is a homoclinic orbit and $|\rho/\lambda|<1$, the condition for this orbit to be of the Shilnikov type, there exists a countable number of infinity Smale horseshoes in the vicinity of the homoclinic orbit.[9] Note that the normal form of Eq. (1) in the D_0 domain is Eq. (2) for $P=Q=R=0$.

In Fig. 12 we show a homoclinic orbit of order-2 (H_2), a solution of Eq. (2), in the coordinates of the eigenvectors of the saddle-focus fixed point. We define two surfaces, $\Sigma_0=\{(x,y,z)\,|\,x^2+y^2<\tilde{r}^2, z=h\}$ and $\Sigma_1=\{(x,y,z)\,|\,y=0, 0<x<\tilde{r}, 0<z<h\}$, also represented in this figure. P_1 is the first crossing of the saddle-focus unstable manifold on the surface Σ_0. Thus, this manifold leaves the z axis on this plane ($z=h$); $\tilde{r}$ gives the limit of Σ_0 and Σ_1.

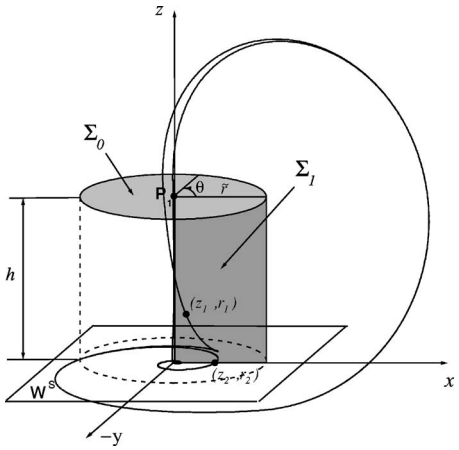

FIG. 12. A H_2 homoclinic orbit in the coordinates of the eigenvectors of the saddle-focus point ($x=y=z=0$). We show the surface Σ_0; on the top of the cylinder at $z=h$ and the surface Σ_1 at $y=0$. P_1 is the point that the unstable manifold of the saddle-focus point crosses the first time on the plane Σ_0; (r_1,z_1) and (r_2,z_2) are successive mapping from Σ_0 to Σ_1 of the homoclinic orbit.

In the region within the cylinder containing surfaces Σ_0 and Σ_1, the dynamics of Eqs. (2) is given by its linearized form

$$\begin{pmatrix} \dot{x} \\ \dot{y} \\ \dot{z} \end{pmatrix} = \begin{pmatrix} -\rho & -\omega & 0 \\ \omega & -\rho & 0 \\ 0 & 0 & \lambda \end{pmatrix} \begin{pmatrix} x \\ y \\ z \end{pmatrix}, \tag{3}$$

where we have chosen $\lambda>0$, a particular solution of Eq. (2), and changed ρ for $-\rho$ (with the new ρ being positive). The solution of Eq. (3) is

$$\begin{pmatrix} x \\ y \\ z \end{pmatrix} = \begin{pmatrix} e^{-\rho t}(x_0 \cos \omega t - y_0 \operatorname{sen} \omega t) \\ e^{-\rho t}(x_0 \operatorname{sen} \omega t + y_0 \cos \omega t) \\ z_0 e^{\lambda t} \end{pmatrix}. \tag{4}$$

Defining $\psi^0:\Sigma_1\to\Sigma_0$, in the cylindrical coordinates, a point (r,θ,z) in Σ_1 is mapped to Σ_0 by

$$\psi^0(r,0,z) = \left(r\left(\frac{z}{h}\right)^{\rho/\lambda}, \gamma, h \right)$$

with $\gamma=(\omega/\lambda)\ln(h/z)$, where we use that $t=(1/\lambda)\ln(h/z)$ [obtained by the solution of $z=h$ in Eq. (4)]. Assuming that there is a primary homoclinic orbit H_1, for the parameter μ_1, the orbit H_2, shown in Fig. 12 for the parameter μ_2, can be thought of as a perturbed orbit around H_1. Thus, we introduce the map $\psi^1:\Sigma_0\to\Sigma_1$ that describes a perturbation around H_1. Then, a point $(r_0,\theta_0,z_0=h)$ in Σ_0 is mapped to Σ_1 in the point $(r_1,0,z_1)$ by

$$\begin{aligned} \psi^1(r_0,\theta_0,h) = [&r_{H_1} + a\Delta\mu_1 + p r_0 \cos(\theta_0+\varphi_1), \ell\Delta\mu_1 \\ &+ q r_0 \cos(\theta_0+\varphi_2)], \end{aligned}$$

where $\Delta\mu_1=\mu-\mu_1$, r_{H_1} represents the coordinate r of the first crossing of H_1 with the surface Σ_1 and we suppressed the coordinate $\theta=0$ of the point in Σ_1. The constants a, ℓ, p,

q, φ_1, and φ_2 depend on the flow. Note that, for $\mu=\mu_1$, $\psi^1(0,0,h)=(r_{H_1},0,0)$, the points $(0,0,h)$ and $(r_{H_1},0,0)$ are in H_1.

Now we apply the same perturbation procedure to study the bifurcation scenario of a subsidiary homoclinic orbit H_{nj} (for μ_{nj}) from a primary homoclinic orbit H_j (for μ_j).

For that, initially, we consider a point $(r_0,\theta_0,z_0=h)$ on the surface Σ_0. From this, as we showed, a point (r_1,z_1) on the surface Σ_1 can be obtained by applying $\psi^1(r_0,\theta_0,h)$. The second point (r_2,z_2) is determined by $\psi^2(r_0,\theta_0,h)=\psi^1\psi^0\psi^1(r_0,\theta_0,h)=\psi^1\psi^0(r_1,z_1)$, so the third point (r_3,z_3) is obtained by $\psi^3(r_0,\theta_0,h)=\psi^1\psi^0\psi^1\psi^0\psi^1(r_0,\theta_0,h)=\psi^1\psi^0(r_2,z_2)$, and so on. So, the nth point (r_n,z_n) is obtained by $\psi^n(r_0,\theta_0,h)$, that is given by

$$\psi^1\psi^0(r_{n-1},z_{n-1})=\begin{cases}\psi^1(r_0,\theta_0,h), & n=1\\ \left[r_1+pr_{n-1}\left(\dfrac{z_{n-1}}{h}\right)^{\rho/\lambda}\cos(\gamma+\varphi_1),z_1+qr_{n-1}\left(\dfrac{z_{n-1}}{h}\right)^{\rho/\lambda}\cos(\gamma+\varphi_2)\right], & n>1.\end{cases}$$

Now we use this map to generate a point (r_{nj},z_{nj}) in Σ_1 from the point $P_1=(0,0,h)$, the first crossing of the unstable manifold on Σ_0. Then, we consider explicitly that a point (r_{nj},z_{nj}) in Σ_1, that is P_1 mapped nj times from Σ_0 to Σ_1, is given by

$$\begin{pmatrix}r_{nj}\\ z_{nj}\end{pmatrix}=\begin{cases}\begin{pmatrix}r_{H_j}+a\Delta\mu_j\\ \ell\Delta\mu_j\end{pmatrix}, & n=1\\ \begin{pmatrix}r_j+pr_{(n-1)j}\left(\dfrac{z_{(n-1)j}}{h}\right)^{\rho/\lambda}\cos(\gamma_{(n-1)j}+\varphi_1)\\ z_j+qr_{(n-1)j}\left(\dfrac{z_{(n-1)j}}{h}\right)^{\rho/\lambda}\cos(\gamma_{(n-1)j}+\varphi_2)\end{pmatrix}, & n>1\end{cases}, \tag{5}$$

where $j\in\mathbb{N}$ is the order of the primary homoclinic orbit, nj is the order of the subsidiary orbits $(n>1)$, $\gamma_{(n-1)j}=(\omega/\lambda)\ln[h/z_{(n-1)j}]$, $\Delta\mu_j=\mu-\mu_j$ and r_{H_j} represents the coordinate r of the jth mapping from Σ_0 to Σ_1 of H_j.

The condition for the existence of any homoclinic orbit H_{nj} is $z_{nj}=0$. Thus a homoclinic orbit H_{nj} is obtained as a solution of Eq. (5) for $z_{nj}=0$ (the orbit returns to the fixed point P_0 after nj turns around P_+). This special solution can be better visualized by introducing two auxiliary functions. To apply that we introduce two auxiliary functions $f=z_{nj}-z_j$, and $g=-z_j$; then the condition $z_{nj}=0$ implies that $f=g$. In Fig. 13 we show the variation of f and g, as a function of z_j, with $n=2$, for two flows, one with the eigenvalues ratio $\delta=|\rho/\lambda|>1$ and the other with $\delta<1$. In the first case, as the Shilnikov condition for the existence of homoclinic orbits is not satisfied, there is no solution for $f=g$ and therefore no homoclinic orbits [Fig. 13(a)]. In the second case [Fig. 13(b)] the Shilnikov condition is satisfied and there are infinite values of $f=g$ and infinite homoclinic orbits H_{2j}. Equivalent results are obtained for $n>2$, therefore, in the limit $z_j\to 0$, the Shilnikov condition implies the existence of an infinity number of order-nj homoclinic orbits accumulating into an order-$(n-1)j$ orbit. Note that the limit $z_j\to 0$ is equivalent to $\Delta\mu_j\to 0$. For the case when $\delta>1$, no subsidiary orbits exist.

The pairwise character of the primary families in Fig. 6, i.e, the existence of two branches in their bifurcation curves, can be inferred from the analytical solutions of Eq. (5) for $z_{nj}=0$, which contains a cosine function.

In Fig. 14 we illustrate the z_{nj} solutions given by Eqs. (5), for $n=1$, $n=2$ and $n=3$, in the neighborhood of μ_j. We show z_j, z_{2j}, and z_{3j} with respect to $\Delta\mu_j=\mu-\mu_j$. The homoclinic orbits H_j, H_{2j}, and H_{3j} exist whenever the coordinates z_j, z_{2j}, and z_{3j} are equal to zero. An important fact in this picture is the number of critical parameters μ_{3j} accumulating into μ_{2j} tending to infinity as $\Delta\mu_j\to 0$ [Fig. 14(b)] and the infinity number of μ_{2j} accumulating into μ_j [Fig. 14(a)]. Moreover, in the parameter interval $\Delta\mu_j$ with a negative z_{2j}, there is no even homoclinic orbit H_{3j} or H_{nj} for $n\in\mathbb{N}$. Thus we identify intervals in the parameter space without any H_n homoclinic orbits.

Therefore, in the accumulation of H_{nj} into $H_{(n-1)j}$ orbits in Fig. 14, we can identify critical parameter sequences μ_{nj}^i with homoclinic orbits H_{nj}^i (of order nj) for each of these parameters. The scaling law describing this accumulation is

$$\frac{\mu_{nj}^i-\mu_{nj}^{i+1}}{\mu_{nj}^{i-1}-\mu_{nj}^i}=\exp^{-\lambda\pi/\omega}, \tag{6}$$

where $n\geqslant 2$ and $j\geqslant 1$; λ and ω are determined by the eigenvalues of the saddle-focus fixed point for the parameter μ_j. The upper index i identifies the sequences of these homoclinic orbits H_{nj}^i appearing in the parameter vicinity of $H_{(n-1)j}$. So, given two consecutive homoclinic orbits with parameters μ_{nj}^i and μ_{nj}^{i+1}, they accumulate for increasing i into $\mu_{(n-1)j}$, where the sequence satisfies $|\mu_{nj}^i-\mu_{(n-1)j}|>|\mu_{nj}^{i+1}-\mu_{(n-1)j}|$. For $n=2$, we have the approach of the subsidiary H_{2j} into the primary H_j. For $n>2$, we have the approach of the subsidiary H_{nj} into the subsidiary $H_{(n-1)j}$, in the

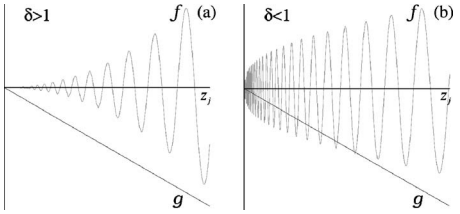

FIG. 13. The f and g functions, for $\delta>1$, not satisfying the Shilnikov condition (a) and for, $\delta<1$, satisfying the Shilnikov condition (b). $f=z_{2j}-z_j$, and $g=-z_j$.

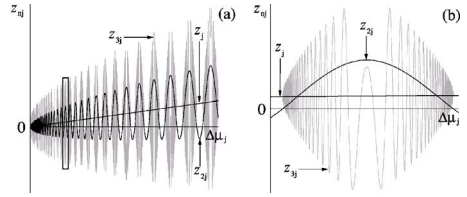

FIG. 14. (a) Solutions z_{nj} in Eq. (5) for $n=1$, $n=2$ and $n=3$. For $z_{nj}=0$, the parameters of homoclinic orbits of order $2j$ and $3j$, accumulate into parameters of the orbit H_j, for the chosen parameters $r_{H_j}=1$, $a=0.1$, $\ell=1$, $p=1$, $q=0.1$, $\rho=1$, $\lambda=2$, $\omega=100$, $\phi_1=1$, $\phi_2=1$, and $h=0.1$. We show $\Delta\mu_j=\mu-\mu_j$. (b) Magnification of the box indicated in (a).

vicinity of the primary H_j. For more details on the derivation of Eq. (6) see Ref. 18. So, while subsidiary orbits accumulate into primary orbits and have always others subsidiary accumulating into them, primaries can only have subsidiaries accumulating into them, and they never accumulate into any other primary.

The one-parameter bifurcation analysis shown in Fig. 14 cannot explain the two-parameter character observed in the homoclinic bifurcations of the Chua parameter space of Figs. 8–10. In particular, the inflection of a d function, with the consequent appearance of other local maximum and minimum, as we vary the parameter β. Such behavior, in the z_{nj} solution of Eq. (5), comes from the second parameter in the two-parameter analysis of this equation due to the coefficient a of the term $a\Delta\mu_j$.

The saddle index $\delta=|\rho/\lambda|$, used in Ref. 17 as the other parameter, is not appropriate here, because, for most primary homoclinic curves, δ does not vary much. For example, the primary homoclinic curves H_6 and H_7 have $\delta<0.2$, as we can see in Fig. 6. On the other hand, the parameter a, to be varied to this work, depends on the flow that is sensitive to the physical control parameter.

In Figs. 15(a)–15(d) we show z solutions of Eq. (5) for four different values of a as we vary $\Delta\mu_j=\mu-\mu_j$ with $z_j \approx 0.06$. In the sequence of Figs. 15(a)–15(c), H_{nj} orbits are created when the local minima of $z_{(n-1)j}$ tend to zero. When $H_{(n-1)j}$ orbit is created there is a finite number of H_{nj} solutions that tend to infinity for $z_j \to 0$ [Fig. 15(d)]. Figure 15(e) shows the theoretical obtained homoclinic bifurcation scenario in the parameter space $\Delta\mu_j$ vs a. In this figure, the filled circles along the family-H_{nj} curves for $a=a_1,a_2,a_3,a_4$ represent $\Delta\mu_j$ values for which the z_{nj} function is zero. This basic geometrical structure represents family-H_{nj} curves accumulating into a family-$H_{(n-1)j}$ curve. Between each pair of family-H_{nj} curves one finds inner and outer accumulations of family-$H_{(n+1)j}$ curves into the below and above family-H_{nj} curves, respectively. These accumulations obey the scaling law described by Eq. (6), and between two pairs of these family-H_{nj} curves no homoclinic orbits H_m, with $m \in \mathbb{N}$, exist. This example of basic structure is of the type within-to-within, where families appear one inside the other.

Due to the within-to-within structure in which family curves appear parallel to other family curves in parameter space, the scaling of Eq. (6) is verified even if one checks the accumulation process in transversal directions that are not strictly perpendicular to two accumulating family curves.

Moreover, we can see an external subsidiary H_{nj} bifurcation curve on the left of Fig. 15(e). This agrees with the H_6 subsidiary curve in Fig. 8 localized externally of the primary H_2. Note that both figures present the within-to-within structures.

The described scenario, with the presented structures and scaling laws, predicts all possible homoclinic bifurcation in the parameter space.

V. CONCLUSIONS

By performing a theoretical normal form analysis of dynamical systems that present Shilnikov homoclinic orbits, we obtain a complete description of homoclinic bifurcations and a scaling law that reveals the basic structures formed by the bifurcation curves in the parameter space of these systems.

We apply this analysis to the Chua circuit and derive numerically all the main features of the homoclinic bifurcation scenario of this system. Thus, we present new high order primary homoclinic orbits in an extended parameter space. This helps us obtain a complete bifurcation curve structure and accumulation process for this system, extending the already known small regions in parameter space, nearby orbits of order one, to the whole parameter space containing homoclinic orbits of any order.

The obtained scenario is a codimension-one of bifurcation curves in the two-parameter space. Thus, we find an infinity number of bifurcation curves, each one representing a type of homoclinic orbit, classified by a natural number named order. These family curves appear organized in a within-to-within structure, in which, given a family curve for orbits of order nj, it can exist an infinity number of other family curves of order $(n-1)j$ accumulating into the order nj family for $\Delta\mu_j \to 0$, being all these curves are close to a primary family curve of order j. The accumulating set of family curves [of order $(n-1)j$ and nj] is referred to as the subsidiary set.

This accumulating scenario of subsidiary family curves into subsidiary family curves as well as subsidiary family curves into primary family curves is governed by a scaling law, which was theoretically derived and numerically verified in the Chua circuit.

Due to the intimate connection between the homoclinic orbits and other sets present in dynamical systems, the basic structure of homoclinic orbit bifurcations should be seen as a skeleton of the parameter space of such sets. Thus, the curve of a family in parameter space could guide one to search to

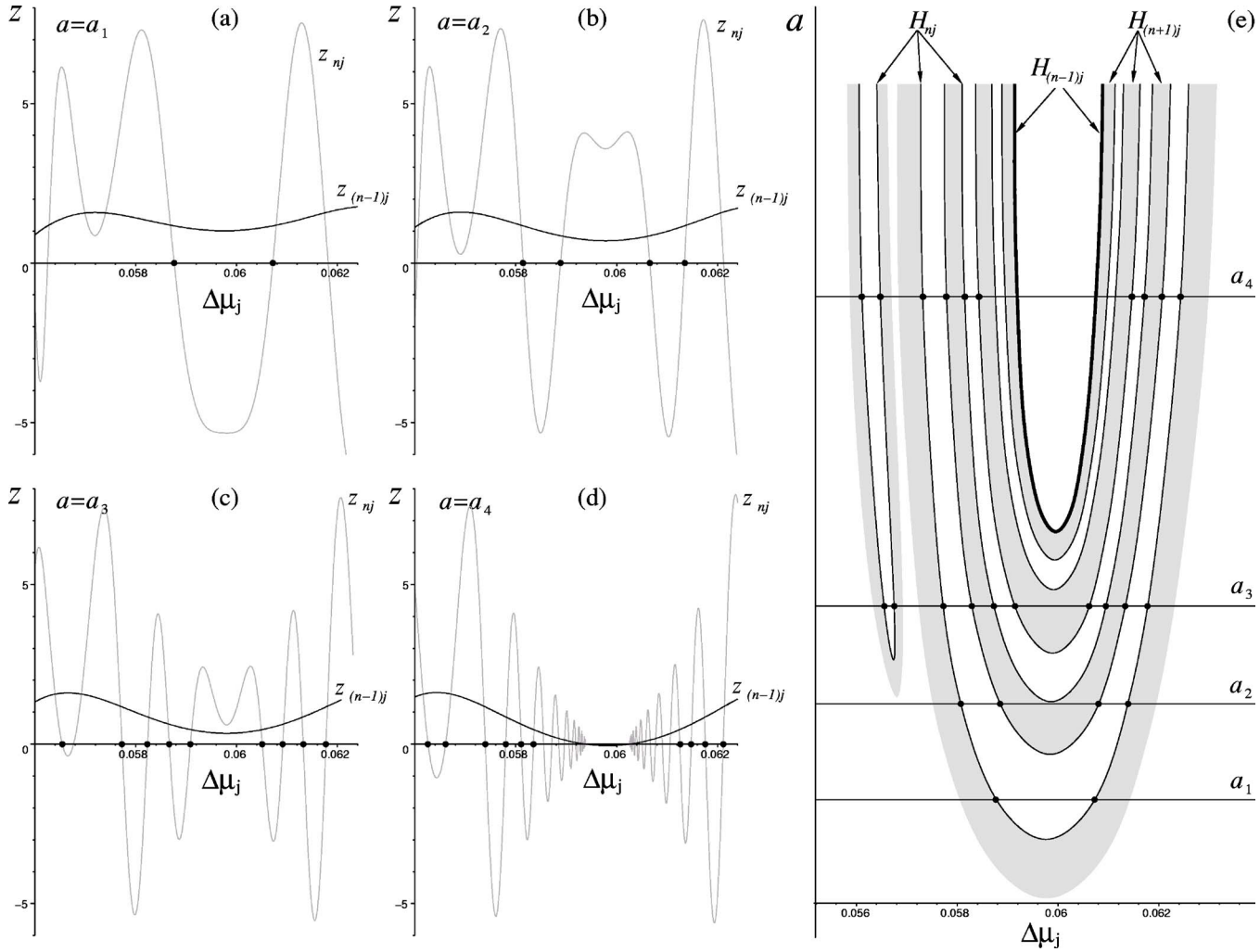

FIG. 15. Solutions z of Eq. (5) for $(n-1)j$ and nj. For $z=0$, we show the accumulation of parameters μ_{nj} (for H_{nj} orbits) into parameters $\mu_{(n-1)j}$, with respect to $\Delta\mu_j$, for $a_1=62$ (a), $a_2=64$ (b), $a_3=68$ (c), $a_4=70$ (d). The chosen parameters are $r_{H_j}=1$, $l=1$, $p=1$, $q=0.1$, $\rho=5$, $\lambda=10$, $\omega=100$, $\phi_1=1.2$, $\phi_2=1$ and $h=0.1$. $\Delta\mu_j=\mu-\mu_j$, where μ_j is the parameter of the primary H_j orbit. In (e) we represent the corresponding basic structure of this homoclinic bifurcation scenario in parameter space $a\times\Delta\mu_j$. In gray are the regions with the inner and outer accumulation of family-$H_{(n+1)j}$ curves into the family-H_{nj} curves indicated by the arrows. In the blank regions there are no homoclinic orbits of the kind H_n. Complementary, the H_{nj} curves are accumulating into the $H_{(n-1)j}$ curves.

particular properties in other coexisting sets, as one varies parameters along that curve. Whenever there is a homoclinic orbit, in a Chua circuit there is an infinity number of periodic orbits and horseshoes associated with it.[22] Therefore, infinity number of periodic orbits and complex horseshoes will be found following the same parameter scaling laws derived in this work. A particular example of such an important connection between the homoclinic bifurcation structure and the parameter space of chaotic attractors in the Chua circuit is an imaginary line beneath all the primary homoclinic orbits very close to the crisis line, in which the Rössler-type attractor bifurcates into the double scroll attractor, through a crisis-induced intermittency.[23] So, this crisis should be associated with the creation of an infinity number of homoclinic orbits and, therefore, an infinity number of horseshoes.

Thus, in this work we extend the previous knowledge about structures of homoclinic bifurcation curves and accumulation of these curves in the parameter space.

ACKNOWLEDGMENTS

We thank the financial support of FAPESP and CNPq.

[1] F. Argoul, A. Arneodo, P. Richetti, J. C. Roux, and H. L. Swinney, Acc. Chem. Res. **20**, 436 (1987).
[2] T. Braun, J. A. Lisboa, and J. A. C. Gallas, Phys. Rev. Lett. **68**, 2770 (1992).
[3] E. M. Izhikevich, Int. J. Bifurcation Chaos Appl. Sci. Eng. **10**, 1171 (2000).
[4] U. Feudel, A. Neiman, and X. Pei, W. Wojtenek, H. Braun, M. Huber, and F. Moss, Chaos **10**, 231 (2000).
[5] D. Parthimos, D. H. Edwards, and T. M. Griffith, Phys. Rev. E **67**, 051922 (2003).
[6] C. S. Zhou, J. Kurths, and E. Allaria, S. Boccaletti, R. Meucci, and F. T. Arecchi, Phys. Rev. E **67**, 015205 (2003).
[7] M. T. M. Koper, P. Gaspard, and J. H. Sluyters, J. Chem. Phys. **97**, 1 (1992).
[8] S. Smale, *Differential and Combinatorial Topology* (Princeton University Press, Princeton, 1963); S. Smale, Bull. Am. Math. Soc. **73**, 747 (1967).
[9] L. P. Shilnikov, Sov. Math. Dokl. **6**, 163 (1965); Math. USSR. Sb. **6**, 427 (1968); Math. USSR. Sb. **10**, 91 (1970).

[10]A. Arneodo, P. Coullet, and C. Tresser, Phys. Lett. **79**, 259 (1980); A. Arneodo, P. Coullet, J. Peyraud, and C. Tresser, J. Math. Biol. **14**, 153 (1982); A. Arneodo, P. Coullet, E. A. Spiegel, and C. Tresser, Physica D **14**, 327 (1985); P. Richetti, and A. Arneodo, Phys. Lett. **109**, 359 (1985).
[11]S. Hasting, SIAM J. Appl. Math. **42**, 247 (1982).
[12]J. W. Evans, N. Fenichel, and J. A. Feroe, SIAM J. Appl. Math. **42**, 219 (1982).
[13]P. Glendinning and C. Sparrow, J. Stat. Phys. **35**, 645 (1984); P. Glendinning and C. Laing, Phys. Lett. A **211**, 155 (1996).
[14]S. Wiggins, *Introduction to Applied Nonlinear Dynamical Systems and Chaos* (Springer, New York, 1996).
[15]P. Gaspard, Phys. Lett. **97**, 1 (1983); P. Gaspard, R. Kapral, and G. Nicolis, J. Stat. Phys. **35**, 697 (1984).
[16]J. A. Feroe, Physica D **62**, 254 (1993).
[17]S. V. Gonchenko, D. V. Turaev, P. Gaspard, and G. Nicolis, Nonlinearity **10**, 409 (1997).
[18]R. O. Medrano-T., M. S. Baptista, and I. L. Caldas (submitted).
[19]R. O. Medrano-T., M. S. Baptista, and I. L. Caldas, Physica D **186**, 133 (2003).
[20]T. Matsumoto and L. O. Chua, IEEE Trans. Circuits Syst. **CAS-32**, 797 (1985).
[21]Given a primary homoclinic orbit of any order-j (H_j), in its parameter vicinity there is the approach of subsidiary order-nj orbits (H_{nj}) into order-$(n-1)j$ orbits ($H_{(n-1)j}$), in the vicinity of H_j ($n,j \in \mathbb{N}$ with $n \geqslant 2$ and $j \geqslant 1$). For $n=2$, we have the approach of the subsidiary H_{2j} into the primary H_j. For $n>2$, we have the approach of the subsidiary H_{nj} into the subsidiary $H_{(n-1)j}$, in the vicinity of the primary H_j.
[22]T. Matsumoto, M. Komuro, H. Kokubu, and R. Tokunaga, *Bifurcations: Sights, Sounds, and Mathematics* (Springer, New York, 1993).
[23]C. Grebogi, E. Ott, and F. Romeiras *et al.*, Phys. Rev. A **36**, 5365 (1987).